

Achieving High Throughput with a Trainable Neural-Network-Based Equalizer for Communications on FPGA

Jonas Ney and Norbert Wehn

Microelectronic Systems Design (EMS), RPTU Kaiserslautern-Landau, Germany

{jonas.ney, norbert.wehn}@rptu.de

Abstract—The ever-increasing data rates of modern communication systems lead to severe distortions of the communication signal, imposing great challenges to state-of-the-art signal processing algorithms. In this context, neural network (NN)-based equalizers are a promising concept since they can compensate for impairments introduced by the channel. However, due to the large computational complexity, efficient hardware implementation of NNs is challenging. Especially the backpropagation algorithm, required to adapt the NN’s parameters to varying channel conditions, is highly complex, limiting the throughput on resource-constrained devices like field programmable gate arrays (FPGAs). In this work, we present an FPGA architecture of an NN-based equalizer that exploits batch-level parallelism of the convolutional layer to enable a custom mapping scheme of two multiplication to a single digital signal processor (DSP). Our implementation achieves a throughput of up to 20 GBd, which enables the equalization of high-data-rate nonlinear optical fiber channels while providing adaptation capabilities by retraining the NN using backpropagation. As a result, our FPGA implementation outperforms an embedded graphics processing unit (GPU) in terms of throughput by two orders of magnitude. Further, we achieve a higher energy efficiency and throughput as state-of-the-art NN training FPGA implementations. Thus, this work fills the gap of high-throughput NN-based equalization while enabling adaptability by NN training on the edge FPGA.

I. INTRODUCTION

In recent years, there has been a remarkable boost in the throughput of communication systems, driven by the rising demand for high-speed data transmission in various applications such as data centers, video streaming, and cloud computing [1]. As a result, peak data rates have increased to 20 Gbit/s for 5G [2] and are expected to reach 1000 Gbit/s for the upcoming 6G standard [3]. Those immense advancements in throughput and data rate come at the cost of increased distortions of the communication signal due to nonlinearities and inter-symbol interference (ISI) e.g. caused by multipath propagation for wireless communication systems or chromatic dispersion (CD) for optical fiber communications. To compensate for those distortions and to achieve reliable communication, more advanced signal-processing algorithms are required.

A promising candidate to tackle the challenges of modern high-throughput communication systems are NN-based

algorithms [4]–[6]. Especially the equalizer, responsible for mitigating the impairments of the communication channel to increase the reliability of the system, is a component that can benefit from the latest advancements of NN research. In particular, NNs have shown remarkable results for channels with nonlinear effects (e.g. high-data-rate optical fiber channels), for which no exact analytical solutions exist for equalization [7], [8].

Besides throughput, key features of next-gen communication systems include flexibility and adaptability [9]. Those aspects are especially critical in the context of changing environmental conditions and transmission characteristics. In general, NN-based systems are well suited to fulfill the strict adaptability requirements. By retraining or fine-tuning the NN, it can adapt to the changing conditions by updating its trainable parameters [10]. However, updating the weights and bias of the NN requires complex optimization algorithms like backpropagation and gradient descent. Performing these algorithms in real time while meeting the high-throughput constraints is challenging on conventional platforms.

In contrast, FPGAs are a promising platform to satisfy the strict throughput and flexibility requirements since they provide a huge parallelism and customizability. For certain low-complex NNs, which are commonly applied in communications, they can even outperform high-performance GPUs in terms of throughput [8]. Additionally, an FPGA design is a first step towards a custom application-specific integrated circuit (ASIC) as used in practical communication systems. Thus, in this work, we present a trainable FPGA implementation of a convolutional neural network (CNN)-based equalizer that satisfies the high-throughput requirements of an optical communication channel while providing retraining capabilities to enable the required adaptability.

In summary, our novel contributions are the following:

- A high-throughput FPGA implementation of a CNN-based equalizer *including* backpropagation featuring an adjustable parallelism for inference and training.
- An optimized one-dimensional convolution (conv1d) layer architecture featuring a custom mapping scheme of two multiplications to a single DSP to increase the achievable throughput on resource-constrained FPGAs.
- An in-depth analysis of the convergence behavior of our CNN-based equalizer for a 20 GBd optical fiber channel.

This work was funded by the German Federal Ministry of Education and Research (BMBF) under grant agreements 16KIS1316 (AI-NET-ANTILLAS) and 16KISK004 (Open6GHuB). Further it was funded by the Carl Zeiss Stiftung under the Sustainable Embedded AI project (P2021-02-009).

- A detailed comparison of our approach to an embedded GPU implementation and to other state-of-the-art FPGA NN training implementations

II. RELATED WORK

In the following, we discuss the most relevant works related to our high-throughput, retrainable FPGA implementation of an NN-based equalizer. First, the state-of-the-art in the field of NN training on FPGA is presented, and afterwards, FPGA implementations of NN-based equalizers are introduced.

A. NN Training on FPGA

In recent years research strongly focused on the acceleration of NN inference using FPGAs [8], [11], [12]. In contrast, for the computationally intensive NN training, GPUs still remain the platform of choice for the majority of applications. Only a few works tackle the challenges of implementing the NN training including backpropagation and weight update on FPGA.

An automatic compiler-based FPGA accelerator for CNN training was presented in [13]. It automatically generates an FPGA-synthesizable hardware description including a novel cyclic weight storage access scheme. As a result, a throughput of up to 479 GOPS is reported. In 2017, Liu et al. proposed an FPGA-based processor for training CNNs [14]. They designed a uniform computation engine design and a scalable framework that exploits parallelism to outperform an Intel i5 central processing unit (CPU) by 10 times regarding processing time. Mazouz et al. proposed an automated CNN back-propagation pipeline generation for FPGA online training in 2021 [15]. A speed-up of 5.8 times was reported as compared to the Nvidia GTX 1050 Ti GPU. An approach to accelerate continual learning was targeted by Tang et al [16]. It enables continuous training on edge FPGAs using a unified channel-level parallelism-based convolutional kernel and a data-reshaping approach. Another work targeting edge devices was published by Hong et al. in 2021 [17]. They designed a lightweight and power-efficient training accelerator for CNNs. With a focus on low-power for mobile and edge computing, an energy reduction of over 4.5 times was reported as compared to existing FPGA accelerators for the MNIST dataset.

FPGA training accelerators targeting communication systems were presented by Ney et al. in 2022 [6] and 2023 [10]. In [6], a trainable NN-based demapper was implemented using a cross-layer-design methodology, and in [10] a novel unsupervised equalizer was presented featuring a fully-pipelined hardware architecture to balance the lifetime of feature maps. However, none of the works is able to satisfy high throughput requirements surpassing $10 \text{ Gbit}\cdot\text{s}^{-1}$.

In summary, some works focus on accelerating the throughput and processing time of NN training on FPGA [13]–[15]. Other works address low-power and low-energy processing for accelerating the training at the edge [6], [10], [16], [17]. However, there is a clear lack of research focusing on high-throughput inference combined with resource-efficient training on FPGA which is mandatory for our application to satisfy

the high-throughput constraints while providing the required adaptability.

B. NN-based Equalization on FPGA

Recent research strongly focuses on enhancing the performance of communication systems using NN-based algorithms [4]–[6]. However, only a few works analyze the implementation complexity on platforms like FPGAs or ASICs which is an essential step for the deployment of practical communication systems.

In [18], the FPGA implementations of recurrent neural network (RNN) and CNN-based equalizers were presented. As a result, the combination of RNN and CNN provided similar performance as the digital back-propagation (DBP) equalizer while achieving a gain compared with the chromatic dispersion compensation baseline. Moreover, the hardware complexity for achieving a 200 Gbit/s and a 400 Gbit/s throughput was evaluated. Another high-throughput FPGA implementation of a CNN-based equalizer was proposed in 2023 [8]. The implementation features optimization from the algorithm down to the hardware architecture. This way, the CNN-based equalizer achieved a bit error rate (BER) one order of magnitude lower than a conventional one while satisfying the throughput requirements of 40 GBd. Kaneda et al. proposed an FPGA implementation of an NN-based equalizer for high-speed passive optical networks (PONs) and showed that the NN-based equalizer outperforms the maximum likelihood sequence estimator (MLSE) equalizer. On FPGA, the impact of fixed-point resolution was analyzed and it was shown that reducing the weight width from 8 to 4 bit resulted in a reduction of 40 % in look-up table (LUT) resources. In [19] an FPGA implementation of a parallel pruned NN equalizer was presented. A significant reduction in BER was demonstrated for a 100 Gbit/s channel. Further, the novel pruning strategy resulted in a 50 % resource reduction without a degradation of communication performance. Huang et al. compared an RNN FPGA implementation with parallel outputs to a fully connected NN for equalization of an intensity modulation with direct detection (IM/DD) channel [20]. They showed that their novel RNN structure can outperform the fully connected NN with the same input size and the same number of training parameters.

To conclude, several works focus on high-throughput FPGA implementations of NN-based equalizers. However, all of the works only include the inference of the NN on the FPGA. Yet, for changing environmental conditions or varying channel characteristics fast adaption of the equalizer is of high importance. Our work focuses on this gap, where adaptation is required while satisfying the high-throughput constraints.

III. SYSTEM MODEL

An overview of the simulated system model of this work is given in Fig. 1. It consists of the transmitter T, the channel model, and the receiver. The symbols \mathbf{x} are transmitted over the channel including the pulse shaping filter \mathbf{h}_{ps} , the channel impulse response \mathbf{h}_{ch} , and the receiver characteristics $f_{\text{rx}}(\cdot)$.

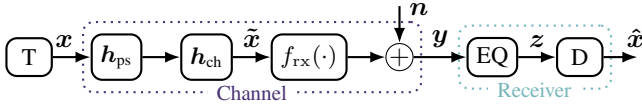


Fig. 1: Model of the communication chain: Data symbols x are sent from a transmitter T over a channel to a receiver R .

At the receiver side, the NN-based equalizer EQ compensates for the distortions introduced by the channel, and a decision D is taken based on the equalizer's output.

A. Communication Scenario

As a potential use-case of our high-speed NN-based equalizer we consider IM/DD PONs. They are usually composed of a point-to-multipoint optical-fiber network such that a single optical line terminal (OLT) is connected to multiple endpoints referred to as optical network units (ONUs). In such systems, increasing data rates lead to severe ISI and nonlinear distortions [21]. To compensate for those distortions equalizers are deployed at the receiver side. Since there is a huge variation in channel conditions for the ONUs [22], it is not practical to provide a unified equalizer with common parameters for each ONU. Instead, each equalizer should be adaptable to the specific channel characteristics, which might also fluctuate over time. For this reason, this use-case fits well to our adaptable NN-based equalization approach.

In particular, we consider an optical channel with IM/DD and pulse-amplitude modulation (PAM) as described in [23]. The square-law detection is modeled by $\tilde{y} = f_{rx}(\tilde{x})$ with $\tilde{y}_i = |\tilde{x}_i|^2$ and distorts the signal nonlinearly while linear distortions are caused by CD given by the frequency response

$$H_{cd}(L_{\text{fiber}}, f) = \exp\left(-\frac{1}{2}\alpha L_{\text{fiber}} + j2\pi^2\beta_2 f^2 L_{\text{fiber}}\right)$$

where L_{fiber} is the fiber length, $\beta_2 = -\frac{\lambda^2}{2\pi c} D_{cd}$ is defined by the wavelength λ , the speed of light c and the fiber's dispersion coefficient D_{cd} ; α is the fiber attenuation.

For our experiments, we consider C-band transmission at $\lambda = 1550$ nm with a length of 35 km, a signal-to-noise ratio (SNR) of 15 dB, $D_{cd} = 17$ ps·nm⁻¹·km⁻¹ and $\alpha \triangleq 0.2$ dB·km⁻¹. Further, we set the transmission rate to 20 GBd since fiber nonlinearities only become significant for high data rates, making nonlinear equalizers like NNs only relevant for high-data-rate scenarios. Thus, achieving the throughput of 20 GBd is a mandatory requirement for our hardware implementation to process the received data in real time.

B. NN Topology

Our NN model of the equalizer employs a 1D CNN architecture, based on the analysis conducted in [8]. Specifically, it consists of two conv1d layers with a kernel size of 9 and a padding of 4 where the first layer is followed by a rectified linear unit (ReLU) activation function. The first layer has 1 input channel, 4 output channels, and a stride of 8, while the second layer has 4 input channels, 8 output channels and a

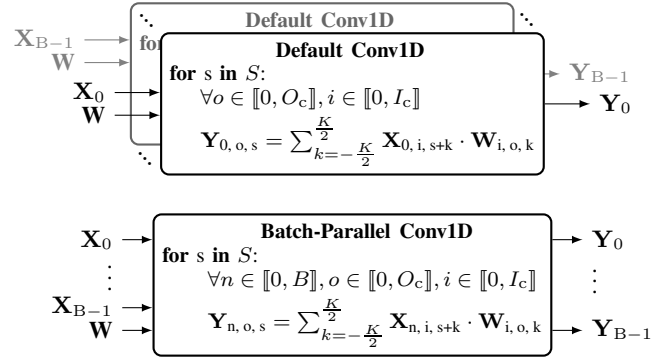


Fig. 2: Comparison of default conv1d and batch-parallel conv1d architecture. All operations in the loops are processed in parallel in one clock cycle.

stride of 2, corresponding to the oversampling factor. This way, 8 samples can be calculated jointly in a single pass of the NN. The NN is designed in a detailed trade-off analysis, similar to the one presented in [8], where further reduction in complexity significantly increases the BER of the system.

IV. HARDWARE ARCHITECTURE

In the following, the FPGA hardware architecture of our CNN-based equalizer is described. In contrast to many previous works, the implementation does not only include the inference of the CNN but also the training is implemented. This enables retraining of the CNN-based equalizer for unseen channels or changing channel conditions. The main focus of the hardware architecture lies on satisfying the high throughput requirements of the optical communication channel which is especially challenging due to the high computational complexity of the backward pass. To reduce the complexity of the hardware implementation, weights, bias, activations, and gradients are represented as arbitrary-width fixed-point numbers. The exact integer and fraction bit widths are determined in a detailed quantization exploration such that neither the training behavior nor the communication performance is sacrificed significantly.

A. Convolutional Layer

Our hardware architecture is based on fully parallelized conv1d layers to maximize the throughput of the implementation. Mathematically, the conv1d layer is expressed as:

$$\mathbf{Y}_{n,o,s} = \sum_{i=0}^{I_c} \sum_{k=-\frac{K}{2}}^{\frac{K}{2}} \mathbf{X}_{n,i,s+k} \cdot \mathbf{W}_{i,o,k} \quad (1)$$

$$\forall n \in \llbracket 0, B \rrbracket, o \in \llbracket 0, O_c \rrbracket, s \in \llbracket 0, S \rrbracket$$

where \mathbf{X} is the input tensor with shape $N \times I_c \times S$, \mathbf{Y} is the output tensor with shape $N \times O_c \times S$, \mathbf{W} is the weight with shape $I_c \times O_c \times K$, I_c gives the number of input channels, O_c gives the number of output channels, K is the kernel size, S is the sequence length, B is the batch size, and $\llbracket 0, N \rrbracket$ gives the set of natural numbers from 0 to N .

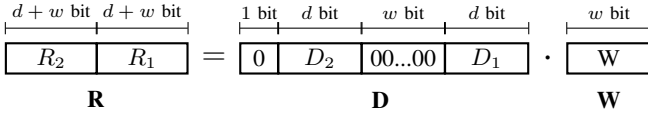


Fig. 3: Mapping of the two multiplication $R_1 = D_1 \cdot W$ and $R_2 = D_2 \cdot W$ to a single DSP

The architecture of our conv1d layer is based on the one presented in [10], which is parallelized on the level of input channels, output channels, and on the kernel level. However, in contrast to [10], where one CNN module is instantiated for each sample in a batch of size B , we include the batch-level parallelism inside the conv1d layer, as shown in Fig. 2. Thus, the weights can be reused for each of the B samples in one batch. This way, the inputs of each instance are first multiplied and accumulated with the same weight before moving the convolutional kernel forward. Eventually, this reduces the resource usage of our architecture, as shown in Sec. V-A. Further, including the batch-parallelism in the conv1d layer enables our custom DSP-mapping scheme, as presented in Sec. IV-B.

B. DSP Mapping

To efficiently utilize the constrained DSP resources of the FPGA, we present a novel approach to map two signed-unsigned multiplications of the second conv1d layer of our CNN to one DSP. As explained in Sec. IV-A, our conv1d layer architecture processes multiple samples of one batch of size B in an unrolled conv1d block. Thus, different inputs are multiplied by the same weight. This allows to reuse each weight B times. In the following, we will refer to the input data $X_{n,i,s+k}$ of equation (1) as D_1 and to $X_{n+1,i,s+k}$ as D_2 where the width of the datatype is given as d . W is short for the weight $W_{i,o,k}$ with width w , and the results of the multiplications are given as R_1 and R_2 with width r . Our goal is to map the two multiplications $D_1 \cdot W = R_1$ and $D_2 \cdot W = R_2$ to a single DSP.

1) *Constraints:* Even with the similar operand W , further constraints must be applied to map the operations efficiently to one DSP. One important constraint is the signedness of the operands. In this case of two unsigned operands, inserting w guard bits between the operands D_1 and D_2 is sufficient. Then the first $d + w = r$ bits of the result R correspond to R_1 and the second r bits correspond to R_2 . However, for our application, W is of type signed since it can also take negative values while D_1 and D_2 are of type unsigned for the second conv1d layer since it's preceded by a ReLU activation function. This problem is slightly different from the one considered in [24], [25], where the common operand is of type unsigned. Therefore, the solution of [24], [25] isn't applicable in our case. Another important constraint is the bit width of the operands. The *DSP48-E2* block of our target FPGA features a 27×18 bit multiplier, thus our combined data input D is limited to 27 bit. As shown in Fig. 3, D consists of D_1 and D_2 , w guard bits, and one leading zero. Thus,

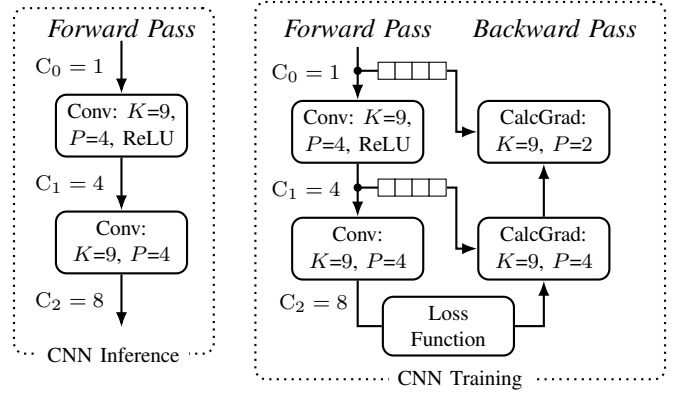


Fig. 4: Comparison of CNN inference and training

$2 \cdot w + d \leq 26$. Experiments showed, that under this constraint a configuration with 6 bit for the weights and 10 bit for the inputs provides the best performance.

In summary, to enable our approach of mapping two multiplications to one DSP the following constraints need to be satisfied:

- A common multiplicand W is used in both multiplication
- W is of type signed, while the other operands D_1 and D_2 are of type unsigned.
- $2 \cdot w + d \leq 26$

2) *Modification:* For the combined multiplication, the result of $D_1 \cdot W$ potentially influences the result R_2 of the multiplication $D_2 \cdot W$. In the case of $W \geq 0$, R_1 is signed-extended with zeros since $\text{Sign}(W) = 0$ and $\text{Sign}(D_1) = 0$. Thus, no overflow is propagated into the calculation of R_2 . However, when $W < 0$, $\text{Sign}(W) = 1$ and $\text{Sign}(R_1) = 1$. Thus, R_1 is signed-extended with ones, which are added to the calculation of R_2 . If we declare ΔR_2 as the difference between the correct result R_2 and the DSP output R_2^* then:

$$\Delta R_2 = R_2 - R_2^* = 111\dots111_2 = -1_{10}.$$

Thus, to get the correct result R_2 , we need to add 1 to R_2^* .

To summarize, the following steps are required to map two signed-unsigned multiplications to a single DSP, as implemented in our hardware architecture:

- 1) get D by concatenating D_1 and D_2 with w guard bits
- 2) extend D with zeros and sign-extend W
- 3) multiply D with W using a single DSP
- 4) the first $d + w$ bits corresponds to the result R_1
- 5) the second $d + w$ bits correspond to R_2^*
- 6) if $W < 0$ then $R_2 = R_2^* + 1$ else $R_2 = R_2^*$

C. Inference and Training Module

In Fig. 4 a high-level overview of the CNN inference and training module is shown. A similar architecture was presented in [10], however in this work, the CNN topology is optimized and reduced in size. Further, a separate CNN inference module is implemented to satisfy the high throughput requirements. The core of the inference module is the highly optimized and

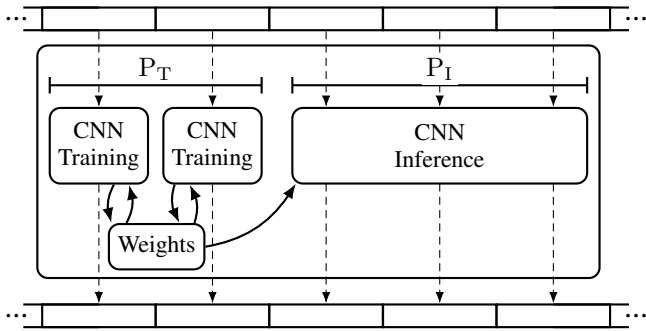


Fig. 5: Parallelism of the training and the inference modules

parallelized conv1d layer. Each layer is connected with an *AXI-Stream* interface to allow for pipelined processing with minimal control overhead. For the training module, forward pass and backward pass are also implemented in a pipeline fashion to balance the lifetime of the feature maps such that the memory footprint is reduced, as described in [10]. Similar to the inference module, the layers of the training module are fully unrolled to enable high-throughput processing. However, batch-parallelism and the custom DSP mapping can only be exploited for the inference module, since the constraints of Sec. IV-B1 are not satisfied by the training module.

D. Parallelism of Inference and Training Module

As shown in Fig. 4, the CNN training is much more complex than the inference since in addition to the forward pass, the loss function, the backward pass, and the weight update need to be implemented. Further, a higher bit width of around 24 bit is required as the values of the gradients are usually very small. Therefore, the resource consumption of the FPGA is much larger for the training module as compared to the inference module with similar parallelism. Thus, in our hardware architecture, we allow for separate degree of parallelisms (DOPs) for inference and training, referred to as P_I and P_T respectively. In particular, P_I is increased by exploiting the batch-level parallelism in the convolutional layer, while P_T is increased by using multiple training modules, as shown in Fig. 5. This way, by increasing P_I while keeping P_T small, we achieve high throughput for the inference, while enabling training of the CNN, even on resource-constraint platforms like FPGAs. It's worth mentioning that in the case of a small P_T , the training is only performed on a subset of the complete input sequence and not all symbols are used for training, however in Sec. V-B we show that stable convergence can be achieved with a low P_T .

To summarize, our novel hardware architecture includes the following features to satisfy the high throughput requirements:

- The conv1d layer is parallelized on the level of input channels, output channels, and on the kernel level.
- Batch-level parallelism is exploited by the conv1d layer of the inference module to enable weight-reuse.
- A custom dsp-mapping scheme is included in the conv1d layer to efficiently use the DSP resources.

- Each layer is implemented as a separate pipeline stage to exploit temporal parallelism.
- Different DOPs are used for inference and training module to balance the resources.

V. RESULTS

In this section, our conv1d hardware architecture is analyzed, the equalizer implementation is evaluated for a high-throughput optical fiber channel, and the FPGA implementation is compared to state-of-the-art and to an embedded GPU implementation.

A. Conv1D Hardware Architecture Analysis

In the following, it is analyzed how three different hardware architectures of the conv1d layer influence the resource utilization on FPGA. The first, commonly used, architecture conv_{def} exploits the parallelism of the convolutional layer in terms of input channels, output channels, and on the kernel level. In this case, batch-level parallelism is introduced by instantiating one CNN instance for each sample in a batch. The second architecture $\text{conv}_{\text{inst}}$ includes the batch-parallelism inside the conv1d layer, as described in Sec. IV-A. The third architecture conv_{map} is the same as $\text{conv}_{\text{inst}}$, extended by our custom DSP-mapping scheme.

In Fig. 6, the utilization of LUT and DSP resources after synthesis is shown for the different architectures. Since our custom mapping scheme can only be exploited by the inference module, we set P_T to 1 and increase P_I until the resources are fully utilized. It can be seen that there is only a minor difference in the LUT usage up to $P_I = 40$. Starting from $P_I = 48$, the LUT resource consumption of conv_{def} and $\text{conv}_{\text{inst}}$ increase significantly, while it grows only slightly for conv_{map} . The reason for this becomes clear when considering the DSP utilization in Fig. 6b. The DSP

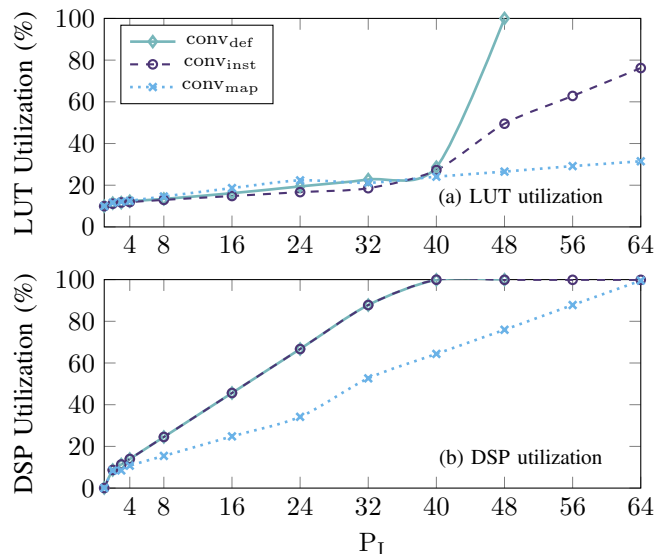


Fig. 6: LUT and DSP utilization of the different conv1d layer architectures on the Xilinx XCVU13P.

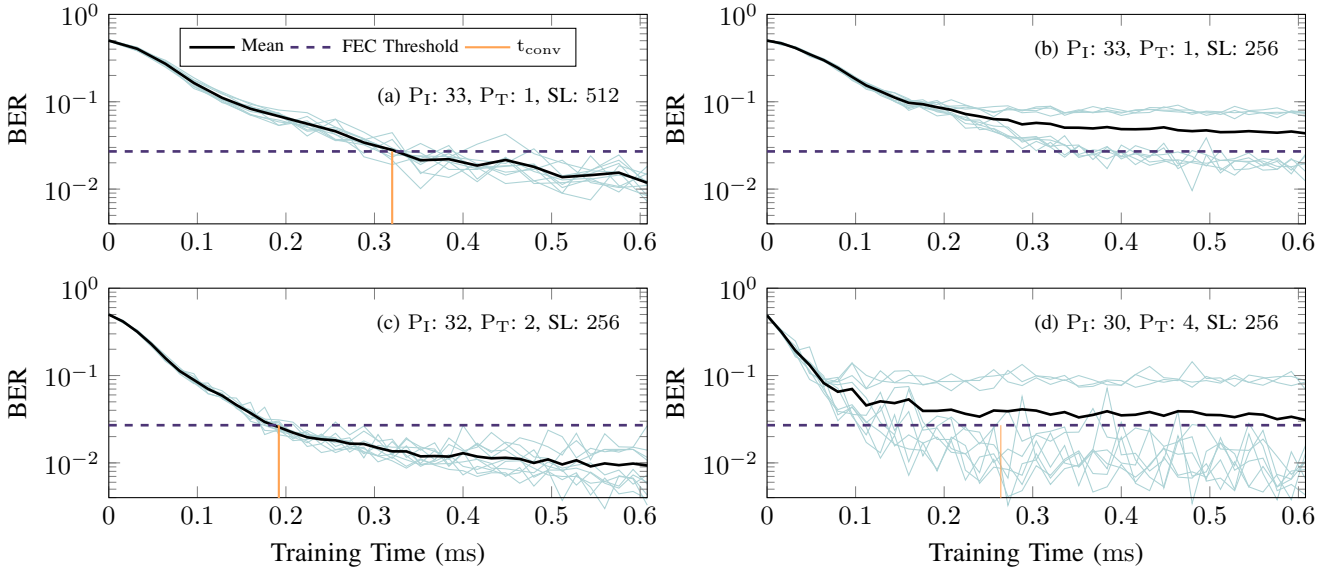


Fig. 7: Convergence behavior of different hardware configurations for the optical fiber channel. Each thin line corresponds to a training run and the thick black line gives the mean of all training runs. The mean convergence time is given by the vertical orange line.

utilization of conv_{def} and $\text{conv}_{\text{inst}}$ increases linearly with P_I with a similar slope. In contrast, the slope of conv_{map} is much smaller since in this case the multiplications of two instances are mapped to a single DSP. Therefore, the DSP resources of conv_{def} and $\text{conv}_{\text{inst}}$ are already fully utilized starting from $P_I = 40$. For that reason, Vivado maps the remaining multiplications to LUTs, which explains the sharp increase seen in Fig. 6a. In summary, the analysis shows that due to our optimized conv_{ld} layer architecture and our custom mapping scheme, the available DSP resources can be used much more efficiently. This leads to a lower LUT utilization, a high number of implementable instances, and eventually increases the throughput achievable by our CNN hardware implementation.

B. Convergence Behavior

In this section, the convergence behavior of our CNN-based equalizer is analyzed for the optical channel described in Sec. III-A. To evaluate the performance and convergence behavior of our hardware architecture, we train different hardware configurations for the described channel model. The main goal of this analysis is to investigate the influence of the sequence length (training symbols per weight-update) and the number of training instances on the convergence time for an unseen channel. The different configurations are implemented on the Xilinx XCVU13P with a clock frequency of 150 MHz, which is the highest frequency achieving timing closure. To satisfy the throughput requirement of 20 GBd with this clock frequency, 34 parallel CNN instances are required, thus $P_I + P_T \geq 34$.

In Fig. 7 the result of this analysis is shown. SL gives the length of each training sequence, corresponding to the number of symbols each training instance processes for one weight-update. The learning rate is set to 0.001 for all configurations since a higher learning rate results in unstable behavior and a lower one increases the training time. We define the convergence time t_{conv} as the training time required to achieve a BER below the forward error correction (FEC) threshold of $2.7 \cdot 10^{-2}$ which corresponds to a low-density parity-check (LDPC) code with 20% overhead [26]. When comparing Fig. 7a and 7b, it can be seen how the sequence length influences the convergence behavior. For the configuration with the largest sequence length of 512 (Fig. 7a), the models of all training runs eventually converge to the FEC threshold, with a mean convergence time of 0.264ms. With a lower sequence length, the convergence behavior becomes more unstable resulting in only 40% of the models converging for a sequence length of 256. One way to reduce the convergence time while maintaining stable convergence is to increase the number of training instances P_T . This way, the weights are updated multiple times based on the gradients of multiple independent sub-sequences. The results of using a different number of training instances can be seen when comparing Fig. 7b, 7c, and 7d. When using two training instances, as shown in Fig. 7c, each training instance performs a weight-update based on the same initial weights. Therefore, a similar behavior as for the configuration with one training instance (Fig. 7a) can be observed although the sequence length is much smaller. However, further increasing P_T results in unstable convergence, as shown in Fig. 7d. Due to the parallel structure of our hardware architecture, the weight-updates of all training

TABLE I: Hardware implementation results

Platform	P_I	P_T	TP (GBd)	t_{conv} (ms)	LUT (%)	DSP (%)
FPGA	33	1	20	0.320	25.18	54.87
	32	2	20	0.192	40.47	57.46
GPU	34	0	$2.6 \cdot 10^{-2}$	—	CNN mode:	Inference
	0	34	$4.7 \cdot 10^{-3}$	910		Training
	8192	0	$7.4 \cdot 10^{-1}$	—		Inference
	0	8192	$1.9 \cdot 10^{-1}$	3500		Training

instances are based on the same initial weights. Thus, each training instance updates the weights with a gradient pointing in a similar direction, resulting in a larger step size and unstable convergence. Experiments showed that even a lower learning rate can't compensate for this effect. To summarize, the fastest stable convergence is achieved by the configuration of Fig. 7c with two training instances and a sequence length of 256, resulting in a convergence time of 0.144 ms.

C. Comparison to Embedded GPU

In Tab. I, we give the FPGA implementation results of the two configurations achieving stable convergence and compare them to the same CNN running on the embedded GPU Jetson AGX Xavier. For the GPU, it is not possible to process the CNN simultaneously in training and inference mode while keeping the weights synchronized. Thus, the model is either set to inference mode or to training mode, where P_I corresponds to the inference batch size and P_T corresponds to the training batch size. In Tab. I it can be seen that increasing P_T from 1 to 2 for the FPGA, increases the LUT utilization by 15% which shows that the computational complexity of the training module is much higher as compared to the inference module. This validates our approach of using a distinct inference module with high parallelism since satisfying the throughput requirements with training modules only would not be feasible. Further, the high throughput is enabled by our custom DSP mapping. With the other conv1d architectures of Sec. V-A the design becomes unrouteable due to high utilization and congestion.

For the GPU we set the batch size to 34, which is the same as for the FPGA, and to 8192 which is the batch size where the throughput of the GPU begins to saturate. It can be seen that even if the model runs in inference mode, without including training, the highest achievable throughput is only 0.19 GBd. This is two orders of magnitude lower than that of the FPGA, which indicates that it is not feasible to satisfy our throughput requirements of 20 GBd with conventional platforms.

Due to the lower throughput, the convergence time t_{conv} is orders of magnitude higher than that of the FPGA. It lies in the order of seconds, which is too high for most practical communication scenarios. For instance, PON requires a re-configuration capacity in the order of μs [21], while a 2 GHz wireless channel with a receiver velocity of $108 \text{ km}\cdot\text{h}^{-1}$ has a coherence time of 2.5 ms [27].

In summary, it can be seen that our custom FPGA architecture is much better suited for the application of high-throughput

TABLE II: Comparison to state-of-the-art

	[16]	[13]	[14]	[17]	[6]	Ours
f_{clk} (MHz)	100	240	200	100	300	150
Batch Size	128	40	16	1	1	34
GOPS	28.15	479	86.12	4.39	5.28	236
TP (Mpixel/s)	0.5	3.4	—	30	49	20 000
Power (W)	6.89	50.47	14.24	0.67	0.57	22.34
η (GOPS/W)	4.09	9.49	6.05	6.55	9.66	10.56

CNN-based equalization than a general purpose GPU. This can be attributed to the fact that GPUs are well suited for the processing of large NNs. In contrast, the computational resources can't be utilized efficiently for NNs of low complexity. In this case, a customized hardware architecture provides much better results.

D. Comparison to State-of-the-Art

In this section, our hardware architecture is compared to other state-of-the-art NN-training FPGA implementations introduced in Sec. II-A. Since there are large variations in the different works (NN topology, target platform, requirements, etc.), for a fair comparison, we mainly focus on the giga operations per second (GOPS) and on the efficiency η given as GOPS/W. Further, we give the throughput in terms of Mpixel/s as a measurement of how many input pixels can be processed per time unit. This allows us to compare the throughput of our 1D-CNN to the two-dimensional CNN architectures of the related works and to the throughput requirements of our channel.

In Tab. II, it can be seen that the highest GOPS is achieved by [13] with 479 while our work provides 236 GOPS. However, higher GOPS does not necessarily result in a higher throughput in terms of pixel/s, since there is a huge difference in the NN topology of the different works. With respect to throughput, our work provides the best results with 20 Gpixel/s, corresponding to 20 GBd for our application. Achieving this throughput is essential to satisfy the communication requirements of our communication channel. This is mainly achieved due to our low-complex CNN topology in combination with our efficient hardware architecture which enables the high inference parallelism. In contrast, the related works mostly focus on the training of much larger CNN topologies making it unfeasible to meet the high throughput requirements.

In terms of efficiency, our work achieves the best result with 10.56 GOPS/W. This can be explained by optimized hardware architecture and our efficient mapping of multiplications to DSP resources.

In summary, the huge variety of different works makes it challenging to provide a fair comparison, however, it becomes clear that our work achieves comparable performance as state-of-the-art hardware accelerators. In particular, for the application of high-throughput equalization, our work fills a gap regarding trainable NN FPGA implementations.

VI. CONCLUSION

In this work, we present an optimized high-throughput FPGA implementation of a NN-based equalizer for communications. The hardware architecture exploits batch-level parallelism in the convolutional layer to enable a custom mapping scheme of two multiplications to a single DSP and provides a variable DOP for the NN inference and the training. The performance of our implementation is demonstrated for an optical fiber IM/DD channel with a data rate of 20 GbD. It is shown that our approach satisfies the high throughput requirements while allowing for adaptation to different channel conditions by training the NN on the FPGA which is validated by a detailed convergence analysis. Further, results show, that our FPGA implementation outperforms an embedded GPU in terms of throughput and provides state-of-the-art performance in terms of energy efficiency as compared to other NN training FPGA implementations. To summarize, our work provides a foundation towards CNN-based equalization on FPGA, which is a crucial step for the development of flexible, high-throughput, next-gen communication systems.

ACKNOWLEDGEMENTS

We sincerely thank Prof. Laurent Schmalen and Vincent Lauinger from the Communications Engineering Lab (CEL) of Karlsruhe Institute of Technology (KIT) for providing the channel model and for the insightful discussions.

REFERENCES

- [1] P. Bayvel, R. Maher, T. Xu, G. Liga, N. A. Shevchenko, D. Lavery, A. Alvarado, and R. I. Killely, "Maximizing the optical network capacity," *Philosophical Transactions of the Royal Society A: Mathematical, Physical and Engineering Sciences*, vol. 374, no. 2062, p. 20140440, 2016.
- [2] K. Kaur and Baliyan, "5G: a new era of wireless communication," *International Journal of Information Technology*, vol. 12, no. 12, 2020.
- [3] N. Rajatheva, I. Atzeni, E. Bjornson, A. Bourdoux, S. Buzzi, J.-B. Dore, S. Erkucuk, M. Fuentes, K. Guan, Y. Hu, X. Huang, J. Hultkonen, J. M. Jornet, M. Katz, R. Nilsson, E. Panayirci, K. Rabie, N. Rajapaksha, M. Salehi, H. Sardeddeen, T. Svensson, O. Tervo, A. Tolli, Q. Wu, and W. Xu, "White paper on broadband connectivity in 6G," 2020.
- [4] A. Zerguine, A. Shafi, and M. Bettayeb, "Multilayer perceptron-based DFE with lattice structure," *IEEE Transactions on Neural Networks*, vol. 12, no. 3, pp. 532–545, 2001.
- [5] M. Schaedler, C. Bluemm, M. Kuschnerov, F. Pittalà, S. Calabrò, and S. Pachnicke, "Deep neural network equalization for optical short reach communication," *Applied Sciences*, vol. 9, no. 21, 2019.
- [6] J. Ney, B. Hammoud, S. Dörner, M. Herrmann, J. Clausius, S. ten Brink, and N. Wehn, "Efficient FPGA implementation of an ANN-based demapper using cross-layer analysis," *Electronics*, vol. 11, no. 7, 2022.
- [7] F. N. Khan, Q. Fan, C. Lu, and A. P. T. Lau, "An optical communication's perspective on machine learning and its applications," *Journal of Lightwave Technology*, vol. 37, no. 2, pp. 493–516, 2019.
- [8] J. Ney, C. Füllner, V. Lauinger, L. Schmalen, S. Randel, and N. Wehn, "From algorithm to implementation: Enabling high-throughput CNN-based equalization on FPGA for optical communications," in *Embedded Computer Systems: Architectures, Modeling, and Simulation*, C. Silvano, C. Pilato, and M. Reichenbach, Eds. Cham: Springer Nature Switzerland, 2023, pp. 158–173.
- [9] H. A. Ahmet Yazar, Seda Dogan Tusha, "6G vision: An ultra-flexible perspective," *ITU Journal on Future and Evolving Technologies*, vol. 1, pp. 121–140, 2020.
- [10] J. Ney, V. Lauinger, L. Schmalen, and N. Wehn, "Unsupervised ANN-based equalizer and its trainable FPGA implementation," 2023.
- [11] Y. Li, Z. Liu, K. Xu, H. Yu, and F. Ren, "A GPU-outperforming FPGA accelerator architecture for binary convolutional neural networks," *J. Emerg. Technol. Comput. Syst.*, vol. 14, no. 2, jul 2018. [Online]. Available: <https://doi.org/10.1145/3154839>
- [12] Y. Duan, S. Li, R. Zhang, Q. Wang, J. Chen, and G. E. Sobelman, "Energy-efficient architecture for FPGA-based deep convolutional neural networks with binary weights," in *2018 IEEE 23rd International Conference on Digital Signal Processing (DSP)*, 2018, pp. 1–5.
- [13] S. Kolala Venkataramanaiah, Y. Ma, S. Yin, E. Nurvithadhi, A. Dasu, Y. Cao, and J.-S. Seo, "Automatic compiler based FPGA accelerator for CNN training," in *2019 29th International Conference on Field Programmable Logic and Applications (FPL)*, 2019, pp. 166–172.
- [14] Z. Liu, Y. Dou, J. Jiang, Q. Wang, and P. Chow, "An FPGA-based processor for training convolutional neural networks," in *2017 International Conference on Field Programmable Technology (ICFPT)*, 2017, pp. 207–210.
- [15] A. Mazouz and C. P. Bridges, "Automated CNN back-propagation pipeline generation for FPGA online training," vol. 18, no. 6, p. 2583–2599, dec 2021.
- [16] Y. Tang, X. Zhang, P. Zhou, and J. Hu, "Ef-train: Enable efficient on-device CNN training on FPGA through data reshaping for online adaptation or personalization," *ACM Trans. Des. Autom. Electron. Syst.*, vol. 27, no. 5, jun 2022. [Online]. Available: <https://doi.org/10.1145/3505633>
- [17] J. Hong, S. Arslan, T. Lee, and H. Kim, "Design of power-efficient training accelerator for convolution neural networks," *Electronics*, vol. 10, no. 7, 2021. [Online]. Available: <https://www.mdpi.com/2079-9292/10/7/787>
- [18] P. J. Freire, S. Srivallapanonndh, M. Anderson, B. Spinnler, T. Bex, T. A. Eriksson, A. Napoli, W. Schairer, N. Costa, M. Blott, S. K. Turitsyn, and J. E. Prilepsky, "Implementing neural network-based equalizers in a coherent optical transmission system using field-programmable gate arrays," 2022.
- [19] M. Li, W. Zhang, Q. Chen, and Z. He, "High-throughput hardware deployment of pruned neural network based nonlinear equalization for 100-Gbps short-reach optical interconnect," *Opt. Lett.*, vol. 46, no. 19, pp. 4980–4983, Oct 2021.
- [20] X. Huang, D. Zhang, X. Hu, C. Ye, and K. Zhang, "Low-complexity recurrent neural network based equalizer with embedded parallelization for 100-Gbits/s Λ PON," *Journal of Lightwave Technology*, vol. 40, no. 5, pp. 1353–1359, 2022.
- [21] G. Simon, F. Saliou, P. Chanclou, L. A. Neto, and H. Hallak Elwan, "50Gb/s TDM PON digital signal processing challenges: Mining current G-PON field data to assist higher speed PON," in *2020 European Conference on Optical Communications (ECOC)*, 2020, pp. 1–4.
- [22] H. H. Elwan, F. Saliou, G. Simon, L. A. Neto, and P. Chanclou, "Towards unified channel equalization to meet transmission requirements for next generation passive optical networks," in *2021 Joint European Conference on Networks and Communications & 6G Summit (EuCNC/6G Summit)*, 2021, pp. 165–169.
- [23] D. Plabst, F. J. García Gómez, T. Wiegart, and N. Hanik, "Wiener filter for short-reach fiber-optic links," *IEEE Commun. Lett.*, vol. 24, no. 11, pp. 2546–2550, 2020.
- [24] D. Nguyen, D. Kim, and J. Lee, "Double mac: Doubling the performance of convolutional neural networks on modern FPGAs," in *Design, Automation & Test in Europe Conference & Exhibition (DATE)*, 2017, pp. 890–893.
- [25] S. Lee, D. Kim, D. Nguyen, and J. Lee, "Double MAC on a DSP: Boosting the performance of convolutional neural networks on FPGAs," *IEEE Transactions on Computer-Aided Design of Integrated Circuits and Systems*, vol. 38, no. 5, pp. 888–897, 2019.
- [26] E. Agrell and M. Secondini, "Information-theoretic tools for optical communications engineers," in *2018 IEEE Photonics Conference (IPC)*, 2018, pp. 1–5.
- [27] M. E. Morocho-Cayamcela and W. Lim, "Accelerating wireless channel autoencoders for short coherence-time communications," *Journal of Communications and Networks*, vol. 22, no. 3, pp. 215–222, 2020.